



HAL
open science

Karst investigations using microgravity and MASW; Application to Orléans, France

Nicole Debeglia, Adnand Bitri, Pierre Thierry

► **To cite this version:**

Nicole Debeglia, Adnand Bitri, Pierre Thierry. Karst investigations using microgravity and MASW; Application to Orléans, France. *Near Surface Geophysics*, 2006, 4 (4), pp.215-225. 10.3997/1873-0604.2005046 . hal-03752337

HAL Id: hal-03752337

<https://brgm.hal.science/hal-03752337>

Submitted on 16 Aug 2022

HAL is a multi-disciplinary open access archive for the deposit and dissemination of scientific research documents, whether they are published or not. The documents may come from teaching and research institutions in France or abroad, or from public or private research centers.

L'archive ouverte pluridisciplinaire **HAL**, est destinée au dépôt et à la diffusion de documents scientifiques de niveau recherche, publiés ou non, émanant des établissements d'enseignement et de recherche français ou étrangers, des laboratoires publics ou privés.

Karst investigations using microgravity and MASW; Application to Orléans, France

Nicole Debeglia*, Adnand Bitri and Pierre Thierry

BRGM-ARN, 3, avenue C. Guillemin, BP6009, 45060 Orléans, France

Received February 2005, revision accepted November 2005

ABSTRACT

An integrated geophysical approach to detecting and characterizing karst structures in an urban environment was applied experimentally to partially explored karst conduits located in Orléans, France. Microgravity was performed to detect voids, in conjunction with multichannel analysis of surface waves (MASW) for the purpose of identifying areas of mechanical weakness.

Microgravity detected negative anomalies corresponding to known conduits and succeeded in identifying the probable extensions of this network in unexplored areas. Control boreholes located on these extensions encountered several levels of water-saturated voids, probably belonging to the shallowest part of the karst system, overlying the main conduits. Buried urban networks, accurately located by ground-penetrating radar (GPR), were shown to have no significant gravity effect. Simulations using the compact inversion approach to characterize the size and density of environmental disturbances confirmed this conclusion. In this context, the gravity method has been shown to be suitable for detecting near-surface (<25 m deep) karst features.

The MASW method, which analyses Rayleigh-wave propagation, can determine the mechanical behaviour of superficial formations and serve as an indicator for subsurface heterogeneities such as voids or fractures. At the Orléans site, MASW provided evidence of perturbed zones superimposed on gravity anomalies, characterized by the appearance of several dispersion modes, velocity inversions and the attenuation of seismic markers. One of these features was characterized by low velocities and was interpreted as an area of mechanical weakness, confirmed by pressure measurements in the boreholes.

Repeated gravity measurements, or time-lapse microgravity, were conducted on the anomalous areas to ascertain gravity reproducibility and detect possible temporal variations due to subsurface mass redistribution that may indicate site instability. A two-year experiment revealed low-amplitude gravity changes that were recorded in the two sensitive zones. However, their significance is still unclear and these changes need to be validated by further repeat experiments.

INTRODUCTION

Shallow karst caves constitute serious hazards for the public and existing constructions, due to the risk of collapse and subsidence that is liable to cause damage to buildings and increase the costs of urban development. Detecting karst features, voids, surficial dissolution, fissuring, alteration and unconsolidated material by geophysical techniques is thus a major challenge for many cities. The city of Orléans, where these tests were carried out, is located some 100 km south of Paris, on the banks of the River Loire, and is built on a highly karstified marly-limestone substratum. As evidence of this, the Loiret springs are amongst the most important karst exurgences in France, and collapse and sinkholes regularly occur in their vicinity. The cavities were also the cause of unforeseen expenses during the construction of a tramway line

and a bridge over the Loire. The geophysical measurements conducted on the Loiret site are integrated into a general approach that aims to assess karst hazards in urban environments (Thierry *et al.* 2004).

Karst systems are characterized by complex geomorphology and hydrology. Voids can take the form of large cavities, superimposed conduits and networks of open fractures or micrometric fissures. Karstification is commonly revealed by surficial features: in the uppermost layer of karstified zones, dissolution by meteoric water can enlarge fissures, thereby creating a zone of rapid infiltration filled with weathered, fractured and unconsolidated material, or epikarst. Epikarst development can cause subsidence (dolines) or collapse phenomena, and results in seasonal perched aquifers. Depending on climatic conditions, the drainage, saturation and physical or geochemical characteristics of the system can vary: the uppermost conduit may or may not

* n.debeglia@brgm.fr

be saturated with water, and some parts of the network may either be filled with unconsolidated sediments or be empty. This complexity produces multiple and time-variable geophysical signatures.

Density and resistivity are known to be very good indicators of the degree of weathering and fissuring of draining or saturated epikarst, and electrical behaviour may be enhanced by the presence of shallow groundwater and strong water circulation. Providing that anthropogenic interference allows their use, microgravity and electrical or electromagnetic imagery are proven methods for indirectly detecting karst systems (Guerin and Benderitter 1995; Kaufmann 2000; Ioannis *et al.* 2002; van Schoor 2002). Ground-penetrating radar (GPR) can also be suitable where soils or argillaceous cover, which absorb radar waves, are absent or highly discontinuous (Al-Fares *et al.* 2002). Unfortunately, the soils in the Orléans region are far too argillaceous for GPR investigation, and the urban setting of the study is unsuitable for electrical imagery methods. Thus, microgravimetry is one of the few methods that could be considered in such an environment, providing that the volume and depth of the voids lend themselves to this technique (Crawford 2000; Beres *et al.* 2001; Rybakov 2001).

However, the use of a combination of geophysical tools is always preferable for obtaining a better-constrained model of karst features. For example, the exploration of a karst network in the Swiss Jura was conducted by combining GPR which

provides a precise image of most surficial voids and structures, with gravimetry, which is sensitive to the presence of deeper and more extensive heterogeneities (Beres *et al.* 2001). Due to the weak penetration anticipated for GPR in this site, a survey coupling microgravity and multichannel analysis of surface waves (MASW), suitable for providing evidence of areas of mechanical weakness (Matthews *et al.* 1996; Ganji *et al.* 1997; Park *et al.* 1998; Leparoux *et al.* 2000; Shtivelman 2002), was undertaken. Several anomalous zones were detected by this approach and validated by control boreholes.

Understanding of the origin of temporal changes in geophysical responses is essential for estimating measurement uncertainties and validating interpretations. Hydrological variations and meteorological conditions are known to influence most methods and, more particularly, gravity (Mäkinen and Tattari 1988; Bower and Courtier 1998; Akasaka and Nakanishi 2000; Harnisch and Harnisch 2002). In active zones, repeated (or time-lapse) microgravity surveying has been used to monitor subsurface mass redistribution associated with the development of sinkholes and to predict impending collapse (Rybakov *et al.* 2001) or to investigate the cause of mine-related subsidence (Branston and Styles 2003). In order to verify the reproducibility of measurements and to try to assess the stability and evolution of low-density areas that have been detected, repeated gravity acquisitions were also conducted on the Loiret site.

KARST DETECTION USING COUPLED GEOPHYSICAL METHODS

The study area is located on either side of a slope that is an ancient terrace on the margin of the Loire alluvial valley (fig. 1). Siliceous and argillaceous alluvia, 5 to 10 m thick, overlie the calcareous Beauce formation of Aquitainian age, in which significant karst dissolution features occur. Karstification has resulted in many surface depressions (avens, sinkholes, dolines) and irregularities in the upper surface of the Beauce formation. Upstream of the Loiret exurgence, in the Parc Floral gardens, karst conduits were partially mapped by cave divers. These conduits, generally around 2 to 3 m wide by 1 to 3 m thick, plunge quite rapidly to depths of 15–20 m or more.

Methodology

Exploration strategy

Gravity modelling of the conduits explored showed that, for an isolated 3-m-wide water-filled gallery at a depth of 15–18 m, a 35-m-wide anomaly with maximum amplitude of about 15 μGal would be expected. This amplitude is higher than the 5–10 μGal uncertainties typical of modern gravimeters. However, the detection capability of the method also depends on the presence of perturbing surficial structures, such as artificial reworking, buried urban lifelines or geological heterogeneities, which might distort or mask the expected signals. A measurement spacing of 5 m was chosen in order to reduce statistical noise and to ensure anomaly detection by a sufficiently large number of nearby stations.

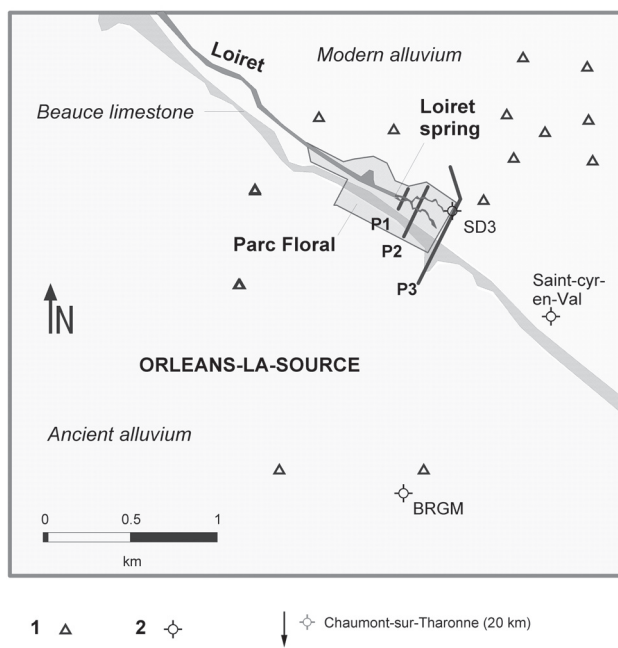


FIGURE 1
Location map of geophysical profiles P1, P2, P3, showing the Loiret River, the karst conduits that were explored and the main geological units. 1: Karst indications (sinkholes, collapses, leaks); 2: piezometers.

Two gravity-calibration profiles were implemented in the Parc Floral, upstream of the Loiret springs, to intersect known conduits (profiles 1 and 2, fig. 1). They are located in a quiet environment but on heterogeneous reworked ground including backfilling material and pavements.

The main profile (profile 3), implemented outside the Parc Floral on a car park and adjacent streets, is perpendicular to the assumed extension of the known karst features. There was a risk that the many urban lifelines (sewers, gas, lighting, etc.) known to be present somewhere along this profile would distort the anomalies. GPR profile measurements were performed to locate these networks more accurately. Along these same profiles, detailed gravity measurements were acquired with a smaller spacing of 2 m in order to determine the gravity effects of the structures identified by GPR and to estimate their potential interference.

Continuous acquisition of multichannel surface-wave data has recently shown great promise as an indicator of near-surface anomalies, such as shallow voids and tunnels, fault zones and changes in fluid distribution (Park *et al.* 1998; West and Menke 2000; Shtivelman 2002). During surface-wave acquisition, the near-surface anomaly will exhibit a variety of signatures. The most common of these is the presence of different phase velocities for the frequencies propagating through the anomaly. Another form can be variations in attenuation characteristics. An anomaly may also be detected by the generation of higher modes (Gucunski and Woods 1991; Park *et al.* 1998): arising from velocity inversion, the energy of higher modes tends to increase for high frequencies (Stokoe *et al.* 1994). The dispersion and attenuation anomalies along the seismic profile can serve as indicators of subsurface discontinuities, such as voids, fractures, etc. Along profile 3, the MASW method was coupled with microgravity in order to detect surficial voids, fracture zones, areas of weakness and drainage pathways that could be associated with karst features.

Microgravity acquisition and processing

Gravity measurements were conducted using automated Scintrex CG3-M and CG5 gravimeters, calibrated on a 100 μGal absolute baseline between Orléans and Sèvres (near Paris). At each station, at least two successive readings were acquired, each consisting of the automatic average of a 1- or 2-minute time series of samples, so as to reduce environmental noise. The stations had links with local base stations, repeated at approximately one-hour intervals, to estimate instrumental drift and minimize its correction. These local bases were referenced to the absolute gravity station of Orléans, located 2 km away and assumed to be stable. This allows comparison with further repeated measurements and the integration of complementary information into the survey. Station elevations were acquired by direct levelling, with accuracy of the order of 1 cm, and the sensor height was read to allow gravity reduction to ground level.

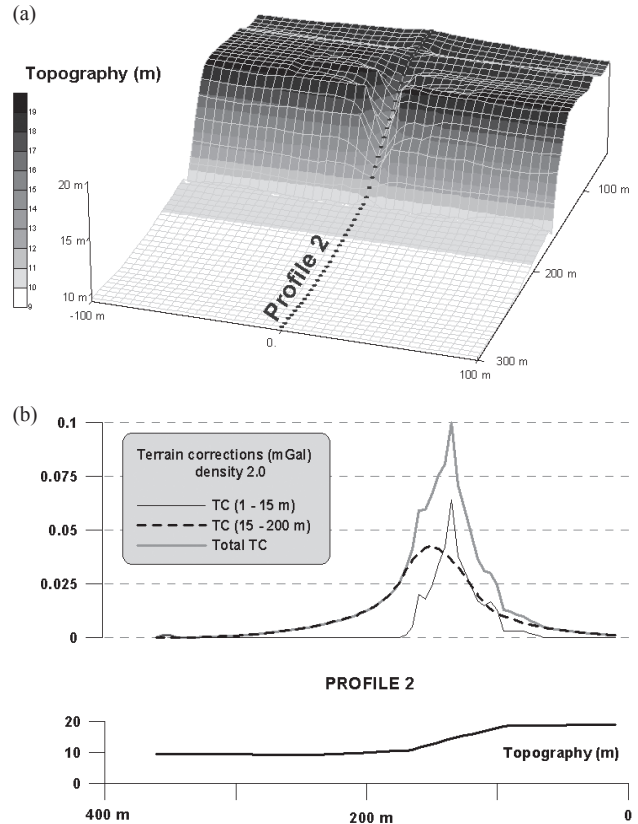


FIGURE 2

(a) Topographic model interpolated from levelling data in the vicinity of profile 2. (b) Terrain corrections: near zones (from 1 to 15 m), intermediate zones (from 15 to 200 m) and total contributions, computed for profile 2.

To determine Bouguer anomalies, readings were corrected for instrumental drift, tides, elevation, latitude and terrain effects, using BRGM proprietary software (Debeglia and Dupont 2002). Accurate tide corrections were obtained using algorithms published by the International Center for Earth Tides (ICET). Optimal Bouguer densities, ranging from 1.6 to 2.0, were estimated for each profile using the Nettleton method. Their variability is the result of changes in the nature of the surficial formations that constitute the topographic relief. Terrain corrections for near zones, corresponding to topographic effects at distances ranging from 1 to 15 m, were computed from elevations estimated by the operator. For intermediate distances ranging between 15 and 200 m from the stations, the corrections were computed using a precise local survey interpolated on a 5-m grid (fig. 2a). The terrain correction reaches 100 μGal on profile 2 (fig. 2b), marked by a sharp slope between the calcareous plateau and the alluvial plain and embedded between steep embankments, 3 to 5 m high. Profile 1 is on a flat area, but at its southern end the slope effect reaches 40 μGal . Along profile 3, the slope is more gradual, and there are no embankments; the terrain effect does not exceed 7 μGal .

Date	Measurement uncertainty (μGal)	Gravimeter
November 23–30, 2001	6.5	CG3 - BRGM
June 25–26, 2002	10.5	CG3 - BRGM
September 25–27, 2002	6.5	CG3 - BRGM
November 15–18, 2002	9.5	CG3 - IPGP
January 29–30, 2003	8.5	CG3 - BRGM
May 27–28, 2003	8.5	CG3 - BRGM
July 29–30, 2003	8.5	CG5 - BRGM (on standard tripod)
December 3–5, 2003	8.5	CG3 - BRGM
December 18–19, 2003	4.5	CG5 - BRGM (on surveyor's tripod)

(northern part of the profile)

TABLE 1

Uncertainty for microgravity observations estimated from statistics on repeated measurements for each successive survey

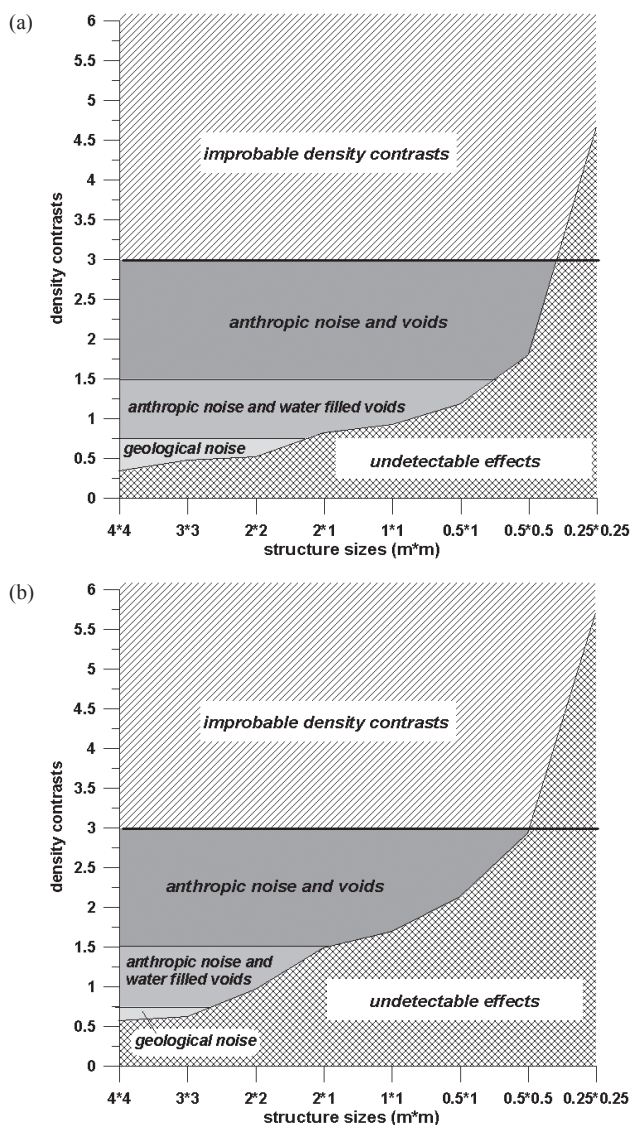


FIGURE 3
Density variations detectable by measurements with (a) 5 μGal and (b) 10 μGal uncertainties.

The uncertainty of Bouguer anomaly estimation depends mainly on gravity readings. About 20% of the stations were revisited during each survey in order to evaluate the repeatability of gravity measurements in the range of 4.5 to 10.5 μGal (table 1). Taking into account levelling and terrain correction errors, the combined standard uncertainty on the Bouguer anomaly was estimated at 7.5 μGal for the first acquisition of profile 3. Locally, due to rugged topography, this uncertainty can reach 25 μGal for some profile 2 stations, but most often it remains smaller than the effect expected for one of the explored karst conduits.

Estimation of environmental disturbances

Detailed GPR and gravity measurements showed that the influence of buried urban networks was negligible on this site, as the few gravity effects observed in correlation with radar anomalies only slightly exceeded the statistical gravity uncertainty (Thierry *et al.* 2004). Except for a settling tank, the source of a 10- μGal anomaly, the conduits identified by GPR did not create significant gravity anomalies.

This result is confirmed by simulations based on gravity inversions (fig. 3a,b). Shallow density heterogeneities are able to mask the expected gravity signals if their effects exceed measurement uncertainty. The size and density-contrast characteristics of such structures were investigated by inverting two synthetic noise profiles with standard deviations set respectively at 5 and 10 μGal . Noise profiles were sampled at a 5-m interval, equal to the measurement spacing, and inverted using a 2.5D compact inversion (Last and Kubik 1983; Guillen and Mennichetti 1984), with the following constraints:

- shallow structures, concentrated in the uppermost 4 m;
- bounds on density contrast ranging between 0 for a void and 3 for metal-reinforced materials;
- maximum compactness of the density distribution and mass concentration involving density-contrast maximization;
- source domain divided into rectangular prisms with elementary cross-section sizes ranging from 4×4 m to 25×25 cm;
- lateral extension of the structures perpendicular to the plane of the cross-section set at 10 m (for shallow structures, this parameter has little influence on the inversion computation);

- acceptable inversion error set at 2% of the anomaly amplitude. Eight inversions were performed with discretization size varying from 25×25 cm to 4×4 m. For each solution of these inversions, the density-contrast range over all the elementary prisms was recorded. Assuming compactness ensures that each anomaly of the noise profile is interpreted by the smallest possible structure, which generally corresponds to an elementary prism. Thus the density-contrast range is statistically representative of the density contrast of elementary size structures. This range increases when the structure size decreases. For instance, with 1×1 m elementary sections, inversion showed that the range of the density contrast must be at least 0.92 to generate an amplitude noise level of 5 μGal, whereas for smaller structures the density-contrast range must be more than 3. Represented on a graph of structure-size versus density-contrast range (Fig. 3a,b), this makes it possible to define the density distributions that can be detected by a survey having a given uncertainty level, or that can distort it.

For a 5 μGal uncertainty survey, a geological noise, defined by a maximum density-contrast variability of 0.75, can be detected if the cross-sectional size of the structures exceeds 2×1 m (fig. 3a), whereas, for a 10 μGal uncertainty survey (fig. 3b), structure size must be at least 3×3 m to be detectable. Structures or backfilling materials including metallic objects, water-filled caves or pipes, corresponding to a density contrast ranging between 0.75 and 1.5, could interfere if their cross-sections exceed 0.5×1 m, for an accuracy of 5μGal. For 10 μGal accuracy, their cross-section must be at least 2×1 m. Voids, empty pipes or metallic objects with density contrasts ranging between 1.5 and 3 could be detected if their cross-section is at least 50×50 cm. Objects having a 25×25 cm cross-section will never be detected.

MASW acquisition and processing

Data were acquired along a line, with most of the site covered by asphalt. To increase the speed and efficiency of MASW data recording and thereby keep acquisition costs down, a new type of multichannel seismic cable has been designed and manufactured. It consists of 24 takeouts at fixed 2-m intervals. Each takeout is attached to a single self-orientating, gimbal-mounted, vertical geophone. To help ensure proper coupling, each gimbal geophone is housed in a heavy casing (~1 kg). To damp the motion of the sensor around its rotational axis, the inside of the casing is filled with viscous oil. The seismic cable is towed behind a vehicle. A 24-channel Geometrics Stratavizor seismograph was used to record and vertically stack four impacts from a 10-kg hammer. The source-to-nearest-receiver offset was 2 m, whilst the source stations were separated by 4 m. Various tests (van der Veen and Green 1998) applying these techniques have demonstrated that high-quality data, comparable to planted spike geophone data, can be acquired with gimbal geophones.

Each 24-trace shot gather was analysed with SIRayD (a proprietary software package of BRGM), facilitating the use of MASW with continuous profiling techniques. The first step consists of determining the dispersion curve, i.e. the phase velocity variation versus frequency. It is calculated by using the slant-stack method in a common-shot gather, followed by a 1D Fourier transform over the intercept time (McMechan and Yeldin 1981; Moktar *et al.* 1988). The transformation of the wavefield into the wavenumber–frequency (v - f) plane can be expressed by

$$U(v, f) = \sum_{i=1}^N C^{-1}(f) A(x_i, f) \exp(j\phi_i) \exp\left(\frac{2\pi jfx_i}{v}\right),$$

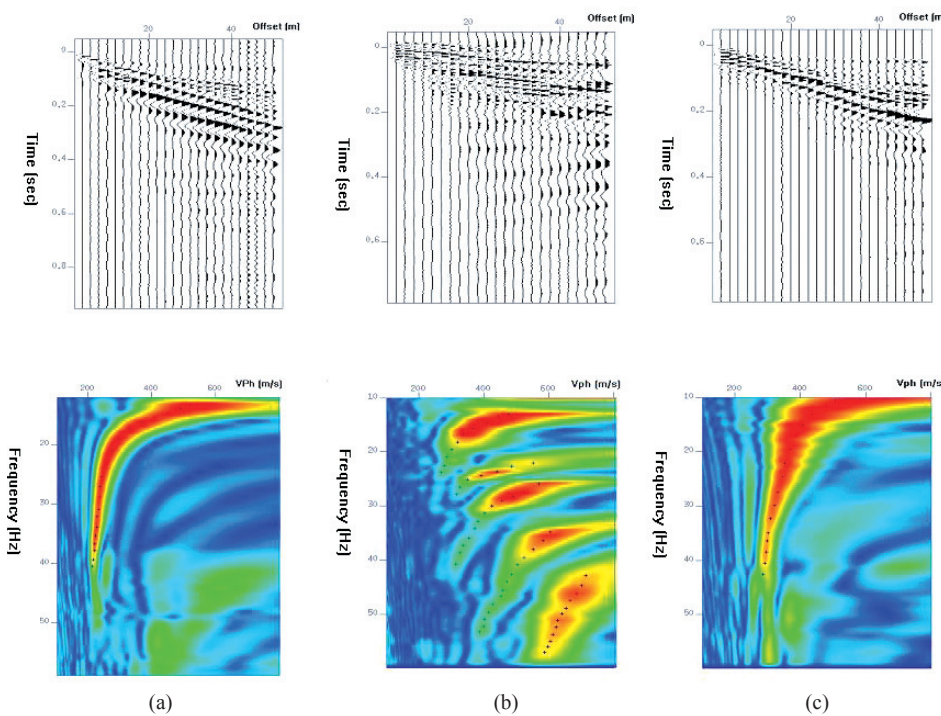


FIGURE 4
MASW shots and the dispersion diagram recorded at the Parc Floral site in (a) the southern, (b) the central and (c) the northern parts of the high-resolution profile.

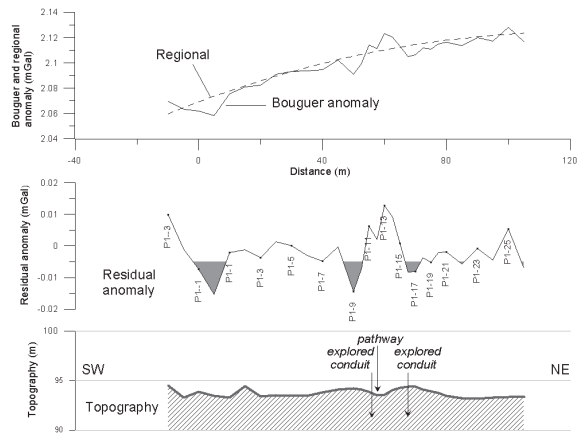


FIGURE 5 Profile 1: Bouguer anomaly, residual anomaly and topography with location of explored conduits and pathway.

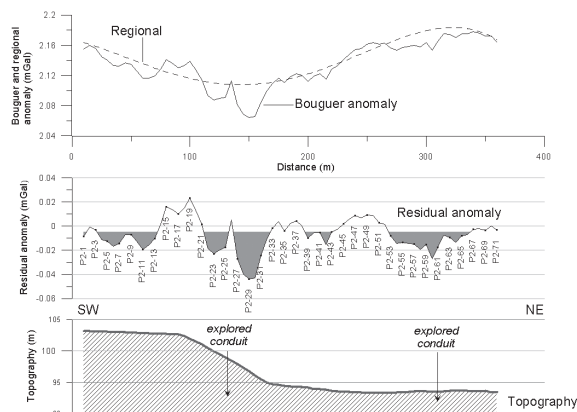


FIGURE 6 Profile 2: Bouguer anomaly, residual anomaly and topography with location of explored conduits.

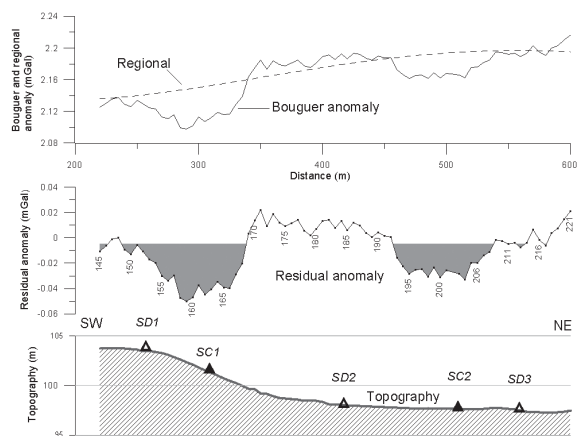


FIGURE 7 Profile 3: Bouguer anomaly, residual anomaly and topography with location of control boreholes.

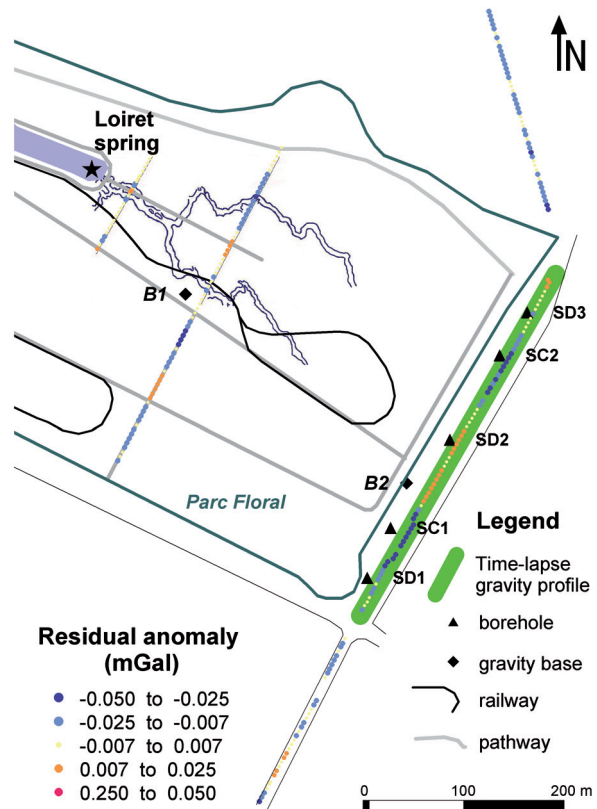


FIGURE 8 Residual gravity anomalies superimposed on the explored karst map, showing the locations of the gravity bases and control boreholes.

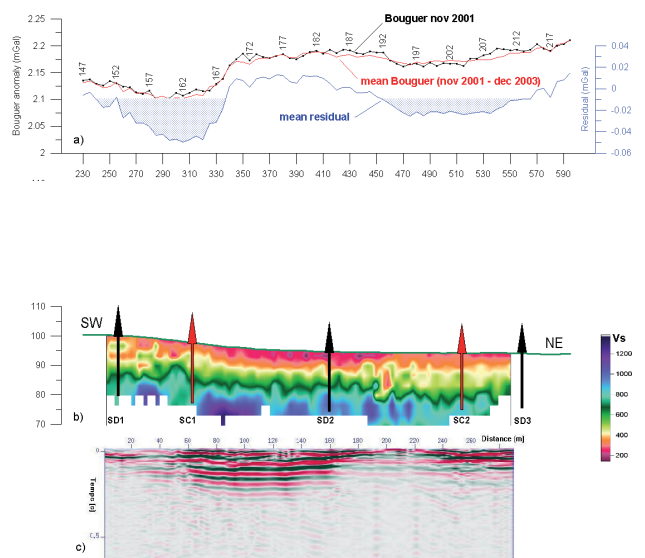


FIGURE 9 High-resolution MASW and microgravity reconnaissance along the central part of Profile 3: (a) gravity anomalies; (b) V_s velocity section; (c) surface-wave image stack.

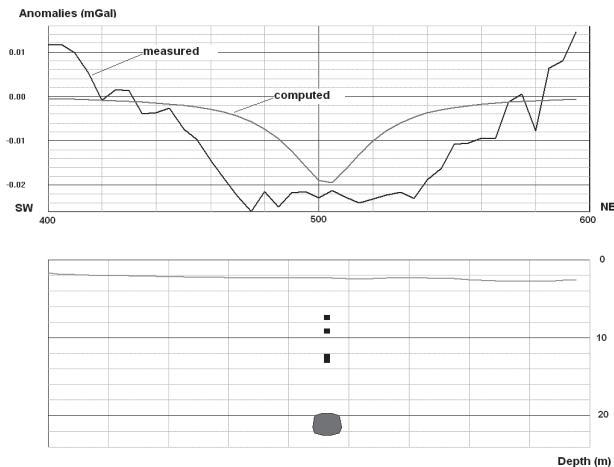


FIGURE 10

Gravity modelling in the vicinity of the SC2 cored borehole: the cumulated effects of three water-saturated voids encountered by SC2 and of a probable deeper conduit cannot totally explain the observed mean residual anomaly.

where $A(xi, f)$ is the amplitude spectrum of the i th trace at distance xi , N is the number of traces in the shot gather, and $C(f)$ is the amplitude spectrum of the first trace. The dispersion curve is directly obtained by picking the maximum values of the modulus of $U(v, f)$ (Fig. 4). Each dispersion curve was individually inverted into a depth versus shear-wave velocity profile. The phase velocity depends on the shear-wave velocity and is insensitive to realistic variations in density and compressional-wave velocity with depth (Gabriels *et al.* 1987; Bitri *et al.* 1998; Xia *et al.* 1999). Different approaches have been proposed for the inversion procedure. The more widely used approach is the linearized iterative least-squares technique (Gabriels *et al.* 1987; Moktar *et al.* 1988; Xia *et al.* 1999; Socco and Strobbia 2004) The linearized iterative least-squares technique used here is adapted from Hermann (1987). A 2D contour plot of the shear-wave velocity field was produced by gathering all the velocity profiles into sequential order, according to half shot station.

In order to facilitate continuous tracing of the dispersion patterns of surface waves along the seismic line, it is convenient to represent them as time sections. The principle is the same as in the seismic-reflection method: the different shots undergo a dynamic correction to remove the offset effects, and then the common-receiver data are stacked. However, the dynamic correction needed for surface waves differs from that used in seismic reflection, because dispersion phenomena must be taken into account (Park *et al.* 1998; Bitri and Grandjean 2004). The resulting stacked section provides an image of the changes in elastic properties of near-surface materials.

Results

Microgravity

The three Bouguer profiles (Figs 5, 6 and 7) displayed a regional trend that was modelled by a bi-dimensional polynomial. The

resulting residual anomalies were superimposed on the map of the karst conduits explored by the divers (Fig. 8). profile 1, situated 50 m from the Loiret Springs, exhibited three negative anomalies, 10 to 15 m wide, with amplitudes of 8 to 15 μ Gal (Fig. 5). Two of them are clearly related to the known conduits. They are separated by a positive anomaly caused by the pathway pavements, denser than the surrounding lawn. Along profile 2, several negative anomalies with amplitudes reaching 20 to 40 μ Gal were detected, two of them being superimposed on known conduits (Fig. 6). On the central part of profile 3, two significant anomalous zones, 60 m wide and with amplitudes of 30 to 50 μ Gal, were detected (fig. 7). The northern one seems to be the extension of one of the explored karsts, and the southern one marks the hill slope, in the continuation of equivalent features of profiles 1 and 2. Further repeat measurements of Profile 3 confirmed these general features, as can be seen on the mean Bouguer and residual curves (Fig. 9). Along profiles 2 and 3, the anomalies are wider and more pronounced than those expected for a single karst conduit having the characteristics of the tunnels explored by the divers. This might be explained by the presence of systems that are more complex than had been anticipated, the anomalies being the sum of the effects of neighbouring conduits and the effects of zones of weakness and fracturation produced by karst circulation. The five control boreholes located along profile 3, validated this interpretation. In fact, the two cored boreholes, SC1 and SC2, situated near the two main negative gravity anomalies, encountered several levels of water-saturated voids at depths between 5 and 20 m. The three other boreholes, SD1, SD2 and SD3, located outside the negative anomalies, did not encounter voids.

At the SC2 borehole, the residual anomalies were modelled by taking into account the three voids, 0.5 to 1.1 m high, detected by the boreholes, at depths of 5, 7 and 10 m (fig. 10). Assuming lateral extents of 2 m, these voids could generate a 6- μ Gal amplitude anomaly. If the effect of the deep explored conduit, not encountered by the borehole, is added, the computed effect reaches 20 μ Gal. However, the computed anomaly is not wide enough to explain the measurements. This modelling showed that other low-density features, i.e. unrecognized voids or unconsolidated and fractured areas, are also present. The width of the low-density zone, perturbed by karst drainage, could be of the order of 60 m.

Multichannel analysis of surface waves (MASW)

The high-resolution MASW profile revealed two perturbed zones superimposed on the gravity anomalies. These zones are characterized by the appearance of several dispersion modes (fig. 4) and by velocity inversions (fig. 9b). Over the same areas, the surface-wave imagery showed attenuation of the continuity of seismic markers (fig. 9c). This signature can probably be related to fracturing and drainage pathways in the epikarst zone.

The shear-wave velocity V_s , ranging from 200 m/s for anthropogenic fills to more than 1000 m/s for massive limestones, were

found to be in good overall agreement with the lithologies encountered by boreholes. A clear difference in the MASW response along the two negative gravity anomalies was observed. For the southern anomalies, high velocity values of up to 700 m/s are present in the upper part of the Beauce formation, corresponding to marl and marly limestones with relatively good mechanical properties. In contrast, in the northern anomaly zone, lower velocity values of around 300–400 m/s were encountered down to a depth of 15 m, indicating an area of weakness approximately 70-m wide. This was confirmed by pressure tests, carried out on the top of the marly limestones, which yielded values for the E-pressure modulus ranging from 1.5 to 7 Mpa. In comparison, in the three boreholes not affected by the gravity anomalies, values ranging from 7 to 35 Mpa were recorded at the same depth and in the same formations. Such incompetent weathered materials, characterized by an elevated depth of refusal, were revealed by their low density and conductivity above palaeokarst features of concentrated karst collapse (Kaufmann 2000).

Discussion

The two boreholes located near the negative gravity anomalies were not deep enough to intersect the main karst conduits, which should not be perturbed, mainly for hydrological reasons. It is not certain whether the gravity method detected these tunnels successfully, as they were buried at depths greater than 20 m under profile 3, although the shallow parts of the system were clearly indicated. The good agreement observed between the karst systems explored and the gravity anomalies revealed by profiles 1 and 2, seems to indicate that the method was successful where the karst features lie at relatively lower depths. However, the gravity response primarily represents epikarst, rather than isolated deep karst conduits, the effect of which is at the limit of the method's detection threshold. As a result, the gravity method appears particularly well suited to locating and characterizing karst systems when karstification is associated with surficial dissolution and fracturing or when the voids are evolving towards a cover-collapse sinkhole.

MASW, which makes it possible to estimate the vertical profile of V_s velocity, constitutes a rapid means of determining the rigidity–depth profiles of surficial formations that can complement pressure tests in boreholes (Matthews *et al.* 1996). In the present study, MASW characterized the mechanical state of the ground in low-density areas and contributed to their interpretation. The delineation of a weak mechanical property area can confirm the interpretation of a negative anomaly as a poorly compacted area where karst voids are prone to collapse, and help to define sensitive zones. In contrast, competent mechanical behaviour can indicate that the gravity lows are related to stable voids or formation anomalies.

TIME-LAPSE MICROGRAVITY EXPERIMENTATION

The MASW survey and control boreholes confirmed that the negative anomalies located along profile 3 can be related to the

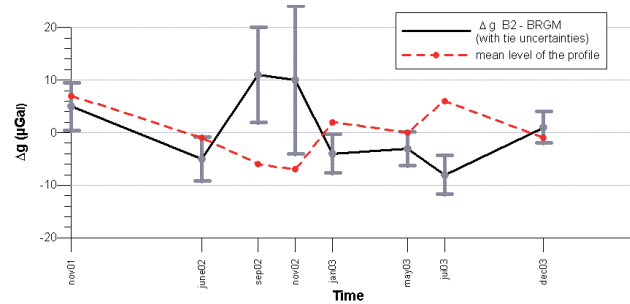


FIGURE 11

Variations of the gravity differences between B2 and BRGM bases compared to the fluctuations of the profile's mean value. Error bars, in grey, correspond to B2-BRGM tie uncertainties.

presence of many drainage pathways and zones of weakness induced by karst circulation. Hence, the central part of profile 3 was selected for a time-lapse microgravity experiment, aimed at searching for possible temporal gravity changes related to potential site instability. Temporal variations may arise from a variety of causes: subsidence, mass displacement (sediments swept along in the karst conduits, sinkhole development and collapses), volume or porosity variations induced by fracturing, soil-moisture variations, etc. This test was also intended to identify the environmental factors liable to influence gravity reproducibility in this context.

Field survey and precision

Gravity measurements were repeated nine times between November 2001 and December 2003 using Scintrex CG3-M and CG5 gravimeters. Most of the time, levelling was also repeated. During each survey, measurements at 15–20% of the stations were repeated to estimate the survey error. G-measurement uncertainties lay in the range of 4.5 to 10.5 μGal (table 1). To account for minor positioning variations, the gravity changes were analysed as simple Bouguer anomaly variations. Also, taking levelling and positioning errors into consideration, the mean quadratic uncertainties on the Bouguer anomaly were estimated at around 9 μGal , varying between 5.5 to 11.5 μGal , depending on the operation. The combined uncertainty s of the Bouguer differences between two repeated measurements, n and m , was estimated from the uncertainties, s_n and s_m , of each survey by

$$s = \sqrt{s_n^2 + s_m^2}.$$

Stability of the local gravity reference

All the measurements were linked to the local reference base station B2, situated at a distance of 25 m from the repeated profile (fig. 8). During each survey, the local base B2 was tied to the absolute base station at Orléans, located on BRGM premises, 2 km from the test site, and assumed to be stable. The uncertainties of these links (Fig. 11) range from 3 to 14 μGal , with a mean value of 6.5 μGal . The fluctuations observed at B2, from $-8 \mu\text{Gal}$

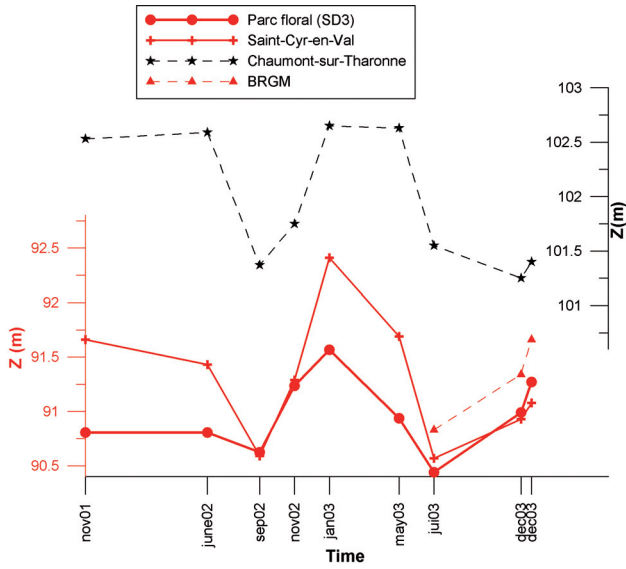


FIGURE 12 Water-table variations at the Parc Floral site (SD3) and at piezometers in the vicinity (Saint-Cyr-en-Val, Chaumont-sur-Tharonne and BRGM).

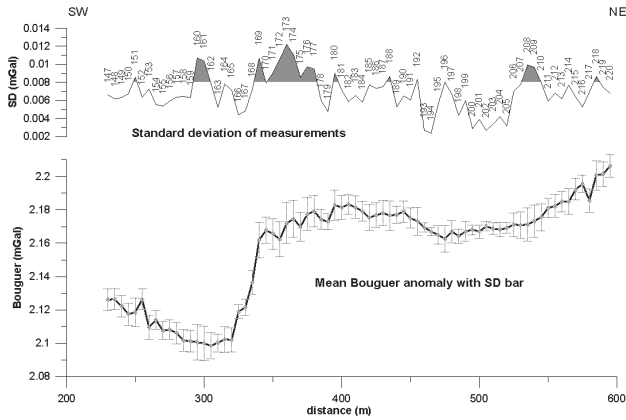


FIGURE 13 Mean Bouguer anomaly and standard deviation (SD) of measurements after eight repeats of measurements between november 2001 and december 2003. The error bar on the Bouguer profile is equal to the SD.

to 11 μ Gal, are comparable to the link uncertainty and are not very significant. To a first approximation, the gravity at B2 was considered to be constant and set at zero, with minor fluctuations of the mean gravity level of the site, of the order of ± 10 μ Gal, remaining possible. Such fluctuations could be responsible for the weak variations in the mean level of the profile (fig. 11).

Influence of hydrological effects

Temporal variations of the groundwater level and soil moisture cause direct gravitational effects liable to affect gravity measurement reproducibility. The Bouguer plate model provides approximations for uniform changes in homogeneous horizontal forma-

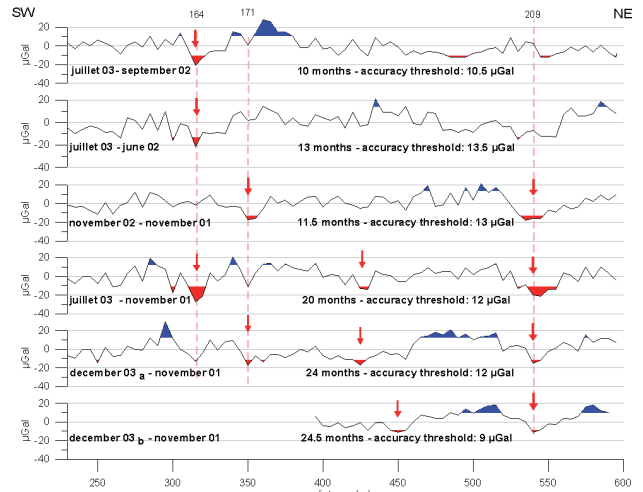


FIGURE 14 Observed changes for several time intervals of between 10 and 24 months. Differences higher than an accuracy threshold equal to the combined uncertainties of the two acquisitions are highlighted in red for gravity decreases and in blue for gravity increases.

tions. Typically, at 10% free-pore volume and saturation, a 1-m rise in groundwater level causes a 4.2- μ Gal increase in gravity and the same variation results from a moisture change of 10% in a 1-m-thick layer of soil (Torge 1989). However, relative gravity measurements will only be affected by local variations due to different hydrological behaviour within the measurement site or between the site and the reference stations.

During each repeat experiment, the water-table level was measured in the SD3 borehole, located on Profile 3, and compared with levels recorded by the nearest piezometers, at Saint-Cyr-en-Val and Chaumont-sur-Tharonne, which are respectively 1 and 20 km from the Parc Floral site (fig. 1). This data displayed similar variations, the most important amplitude discrepancies being recorded between SD3 and Saint-Cyr-en-Val and amounting to 85 cm in November 2001 and January 2003 (fig. 12). Such differences should involve weak gravity effects, of the order of 7.1 μ Gal, for 20% porosity, for example. However, it is unlikely that larger piezometric variations occur locally inside the survey area or between the site and the reference station. the water-table levels recorded on or after July 2003 in a borehole located near the BRGM base station are, in fact, very similar to those of the SD3 piezometer (Fig. 12).

More significant local gravity changes can be caused by temporal or spatial variations in the saturation or moisture of the uppermost soils, above the water-table level, which were recorded at depths ranging between 2.5 and 3.7 m during these tests. Rapid 2.5D modelling showed that a 20% saturation variation in a 3-m-thick by 30-m-wide surficial layer, which could be caused by variations in drainage characteristics according to meteorological conditions, could be expected to produce a gravity change of 20 μ Gal.

Results and discussion

Data were first analysed by comparing the temporal variability of the observed Bouguer anomaly with the estimated uncertainty of measurements (Fig. 13). The mean Bouguer profile resulting from the nine repeat experiments is depicted with a confidence interval corresponding to the standard deviation (SD) of the repeat measurements. On the SD curve, the three areas, where the SD is higher than the mean measurement uncertainty of $9 \mu\text{Gal}$, are indicated by grey cross-hatching. The local base B2 is situated near station 172, very close to the area where the highest changes occur. This possible instability of this part of the site supports the assumption of weak temporal changes in the mean profile level due to B2 variability (fig. 11). Consequently, all the profiles were shifted to a zero mean level, thereby reducing the scattering of repeated measurements. However, it still is higher than the uncertainty on the part of the profile lying between stations 160 and 174.

The shifted data were then represented as time-lapse differences for several time intervals ranging from 10 to 24.5 months. Variations higher than the combined uncertainties of the two surveys are highlighted in red for gravity decreases and in blue for gravity increases (fig. 14). These variations are weak and are limited to the range of $\pm 30 \mu\text{Gal}$. The gravity increases do not clearly correlate spatially from one interval to the other. In contrast, a tendency towards gravity decrease is indicated by several time-lapse differences, mainly at stations 164 and 209. These points are inside the two anomalous areas detected by MASW and gravity, and are close to the boreholes that encountered shallow voids. These time-lapse anomalies could accordingly be related to karst evolution, such as the displacement of unconsolidated sediments, drainage variations or the upward migration of voids. However, with regard to the southern gravity low, this last cause seems unlikely if we refer to the high velocity values observed by MASW that indicated materials with relatively good mechanical properties. In contrast, the size and intensity of the gravity anomaly and the MASW disturbances involve the presence of numerous fractures and open voids in which sediments can be swept away and seasonal drainage variations can occur. More time-lapse experiments with a longer time interval between repeated measurements are planned in order to validate these results and refine interpretations.

CONCLUSION

Microgravity and MASW coupling is a promising approach to detecting and characterizing karst structures in urban environments, the two methods being complementary in depth of investigation and origin of detected anomalies. Microgravity, conducted with close spacing and careful implementation in order to ensure high resolution and accuracy, remains one of the methods best suited to the detection of voids in the uppermost 20 metres, even when these voids are relatively small. Its weakness is the ambiguity of its interpretation. MASW, which is sensitive to the soil stiffness profile, helps to reduce these ambi-

guities by characterizing the mechanical behaviour of the gravity-anomalous zones, and thereby minimizing the extent and cost of mechanical controls. In view of this advantage, the integration of MASW, a technique that is totally non-intrusive, rapid and inexpensive, will always be an asset to the project.

The time-lapse experiment provided evidence of low-amplitude gravity changes that appear to be related to karst evolution. However, further repeats of the experiment will still be necessary to validate and understand them. These tests brought to light the difficulties involved in implementing and interpreting gravity monitoring applications in this context. The frequent recording of weak effects requires accurate difference measurements and precise corrections. Temporal variations may be caused by a variety of phenomena, more or less directly related to karst systems. All these causes should be investigated before a conclusion can be reached concerning the risk of sinkhole development. Moreover, the frequency of repeating the measurements should be adapted to the rate and amplitude of the changes under investigation; these are unfortunately poorly known.

ACKNOWLEDGEMENTS

We thank the divers of the SSL (Spéléologie Subaquatique du Loiret) for having made available their topographic surveys of the main karst conduits. We also thank the Colorado School of Mines for putting the SU package at geophysicists' disposal in freeware (Cohen and Stockwell 1997). We are very grateful to one of the reviewers for their helpful comments. This work was supported by BRGM research program PDR04ARN80.

REFERENCES

- Akasaka C. and Nakanishi S. 2000. Correction of background gravity changes due to precipitation: Oguni geothermal field, Japan. *Proceedings of World Geothermal Congress, Kyushu - Tohoku, Japan*, paper no. R0338.
- Al-Fares W., Bakalowicz M., Guerin R. and Duckan M. 2002. Analysis of the karst aquifer by means of a ground penetrating radar (GPR) - example of the Lamalou area (Hérault, France). *Journal of Applied Geophysics* **51** (2-4), 97-106.
- Beres M., Luetscher M. and Olivier R. 2001. Integration of ground-penetrating radar and microgravimetric methods to map shallow caves. *Journal of Applied Geophysics* **46**, 249-262.
- Bitri A., Le Begat S. and Baltassat J.M. 1998. Shear wave velocity determination of soils from in-situ Rayleigh wave measurements. *Proceedings of 4th EEGS Meeting, Barcelona, Spain*, pp. 503-506.
- Bitri A. and Grandjean G. 2004. Suppression of guided waves using the Karhunen-Loève transform. *First Break* **22**, 27-29.
- Bower D.R. and Courtier N. 1998. Precipitation effects on gravity measurements at the Canadian absolute gravity site. *Physics of the Earth and Planetary Interiors* **106**, 353-369.
- Branston M.W. and Styles P. 2003. The application of time-lapse microgravity for the investigation and monitoring of subsidence at Northwich, Cheshire. *The Quarterly Journal of Engineering Geology and Hydrogeology* **36**(3), 231-244.
- Cohen J.K. and Stockwell J.W.Jr. 1997. *CWP/SU: Seismic Unix. A Free Package for Seismic Research and Processing*. Center for Wave Phenomena, Colorado School of Mines, Golden, CO.

- Crawford N.C. 2000. Microgravity investigations of sinkhole collapses under highways. /Proceedings of the 1st International Conference on the Application of Geophysical Methodologies to Transportation Facilities and Infrastructures, Dec. 11–15, St Louis, Missouri, USA/, 13p.
- Debeglia N. and Dupont F. 2002. Some critical factors for engineering and environmental microgravity investigations. *Journal of Applied Geophysics* **50**, 435–454.
- Gabriels P., Sneider R. and Nolet G. 1987. In-situ measurements of shear wave velocity in sediments with higher mode Rayleigh waves. *Geophysical Prospecting* **35**, 187–196.
- Ganji V., Gucunski. N. and Maher A. 1997. Detection of underground obstacles by SASW method- numerical aspects. *Journal of Geotechnical and Geoenvironmental Engineering* **123**, 212–219.
- Gucunski N. and Woods R.D. 1991. Use of Rayleigh modes in interpretation of SASW test. *Proceedings of 2nd International Conference on Recent Advances in Geotechnical Earthquake Engineering and Soil Dynamics, St. Louis, USA*, pp. 1399–1408.
- Guerin R. and Benderitter Y. 1995. Shallow karst exploration using MT-VLF and DC resistivity methods. *Geophysical Prospecting* **43**, 635–653.
- Guillen A. and Mennichetti V. 1984. Gravity and magnetic inversion with minimization of a specific functional. /*Geophysics*/ *49*, 1354–1360.
- Harnisch M. and Harnisch G. 2002. Seasonal variations of hydrological influences on gravity measurements at Wettzell. *Bulletin d'Informations des Marées Terrestres* **137**, 10849–10861.
- Hermann R.B. 1987. *Computer Programs in Seismology*. Saint-Louis University, USA.
- Ioannis F.L., Filippou I.L. and Bastou M. 2002. Accurate subsurface characterization for highway applications using resistivity inversion methods. *Journal of Electrical and Electronics Engineering*, Special Issue, October 2002, 43–55.
- Kaufmann O. 2000. *Les effondrements karstiques du Tournaisien : genèse, évolution, localisation, prévention*. Thèse 3ème cycle, Faculté Polytechnique de Mons (Belgique).
- Last B.J. and Kubik K. 1983. Compact gravity inversion. /*Geophysics*/ *48*, 713–721.
- Leparoux D., Bitri A. and Grandjean G. 2000. Underground cavity detections: a new method based on seismic Rayleigh waves. *European Journal of Environmental and Engineering Geophysics* **5**, 33–53.
- Mäkinen J. and Tattari S. 1988. Soil moisture and groundwater: Two sources of gravity variations. *Bulletin d'Informations des Marées Terrestres* **62**, 103–110.
- Matthews M.C., Hope V.S. and Clayton R.I. 1996. The use of surface waves in the determination of ground stiffness profiles. *Geotechnical Engineering* **119**, 84–95.
- McMechan G.A. and Yedlin M.J. 1981 Analysis of dispersive waves by wave field transformation. *Geophysics* **46**, 869–874.
- Moktar T.A., Herrmann R.B. and Russel D.R. 1988. Seismic velocity and Q model for the shallow structure of the Arabian shield from short-period Rayleigh waves. *Geophysics* **53**, 1379–1387.
- Park C.B., Xia J. and Miller R.D. 1998. Ground roll as a tool to image near-surface anomaly. 68th SEG Meeting, New Orleans, USA, Expanded Abstracts, 874–877.
- Rybakov M., Goldshmidt V., Fleischer L. and Rotstein Y. 2001. Cave detection and 4-D monitoring: a microgravity case history near the Dead Sea. *The Leading Edge* **20**, 896–900.
- van Schoor M. 2002. Detection of sinkholes using 2D electrical resistivity imaging. *Journal of Applied Geophysics* **50**, 393–399.
- Shivelman V. 2002 Surface wave section as a tool for imaging subsurface inhomogeneities. *European Journal of Environmental and Engineering Geophysics* **7**, 121–138.
- Socco L.V and Strobbia C. 2004. Surface-wave method for near-surface characterization: a tutorial. *Near Surface Geophysics* **2**, 165–185.
- Stokoe K.H, Wright G.W., James A.B. and Jose M.R. 1994. Characterisation of geotechnical sites by SASW method. In: *Geophysical Characterisation of Site*, ISSMFE Technical Committee # 10 (ed. R.D Woods), Oxford Publishers, New Delhi.
- Thierry P., Debeglia N. and Bitri A. 2004. Geophysical and geological characterisation of karst hazards in urban environments: application to Orléans (France). *Bulletin of Engineering Geology and the Environment* **64**(2), 139–150. Published on line, 21 October, 2004.
- Torge W. 1989. *Gravimetry*. Walter de Gruyter, Berlin.
- van der Veen M. and Green A.G. 1998. Land streamer for shallow seismic data acquisition: Evaluation of gimbal-mounted geophones. *Geophysics* **63**, 1408–1413.
- West M. and Menke W. 2000. Fluid-induced changes in shear velocity from surface waves. *Proceedings of SAGEEP 2000*, pp. 21–28.
- Xia J., Miller R.D. and Park C.B. 1999. Estimation of near-surface shear-wave velocity by inversion of Rayleigh wave. *Geophysics* **64**, 691–700.

Seismic Accessories

Land Streamers—for efficient seismic surveys

Wall-Lock Borehole Geophones

Rollalong Switches 24, 48 & 96 channel

Geostuff
<http://www.geostuff.com>
 Tel 530-274-4445, fax 530-274-4446